Nanoscale Research Letters

NANO EXPRESS Open Access

Experimental and Theoretical Studies of Mo/Au Schottky Contact on Mechanically Exfoliated β-Ga_2O_3 Thin Film

Zhuangzhuang Hu, Qian Feng*, Zhaoqing Feng, Yuncong Cai, Yixian Shen, Guangshuo Yan, Xiaoli Lu, Chunfu Zhang, Hong Zhou, Jincheng Zhang* and Yue Hao

Abstract

We studied the reverse current emission mechanism of the Mo/β-Ga_2O_3 Schottky barrier diode through the temperature-dependent current-voltage (I-V) characteristics from 298 to 423 K. The variation of reverse current with the electric field indicates that the Schottky emission is the dominant carrier transport mechanism under reverse bias rather than the Frenkel–Poole trap-assisted emission model. Moreover, a breakdown voltage of 300 V was obtained in Fluorinert ambient with an average electric field of 3 MV/cm in Mo/β-Ga_2O_3 Schottky barrier diode. The effects of the surface states, on the electric field distribution, were also analyzed by TCAD simulation. With the negative surface charge densities increasing, the peak electric field reduces monotonously. Furthermore, the Schottky barrier height inhomogeneity under forward bias was also discussed.

Keywords: β-Ga_2O_3 Schottky diode, Carrier transport mechanism, Reverse bias, Schottky emission, Breakdown voltage

Background

Recently, the ultra-wide bandgap semiconductor β-Ga_2O_3 has attracted lots of interests for its excellent characteristics, such as high chemical stability, large direct wide band gap of 4.8–4.9 eV, high theoretical breakdown electric field (E_{BR}) of 8 MV/cm, and high Baliga's figure-of-merit of 3400, which is about ten times larger than that of SiC and four times larger than that of GaN [1–3]. The combination of all these properties with the high quality, large area, and cost-effective β-Ga_2O_3 substrate grown by melt growth techniques makes β-Ga_2O_3 a preferred material for high-voltage and high-power electronics applications [4–9]. As a promising electronic device, β-Ga_2O_3 Schottky barrier diodes (SBD) were fabricated with various anode electrode metals, including Cu [8], Pd [10], Pt [5, 6, 11–13], Au [10, 14], Ni [13, 15–18], and TiN [12], and its forward and reverse electrical characteristics, such as the specific on-resistance, I_{on}/I_{off} ratio, barrier heights, reverse leakage current, and breakdown voltage, were comprehensively investigated. The inhomogeneous Schottky barrier height and non-saturating reverse bias current were reported in β-Ga_2O_3 SBDs [6, 8, 11, 18, 19] while much less information was known about carrier transport mechanism under reverse bias, which is essential for the breakdown voltage enhancement.

In addition, there is no investigation that has been made to analyze the emission mechanisms of Mo/β-Ga_2O_3 contact. If there are some traps or defects in the β-Ga_2O_3 substrate, the leakage current will be found to be in agreement with the Frenkel–Poole emission model, and the reverse current is the emission of electrons from a trapped state near the metal-semiconductor interface. Otherwise, the main process in reverse current will be dominated by the Schottky emission that the electrons over the Schottky barrier result in a reverse current. β-Ga_2O_3 crystal also has one unique property, a large lattice constant of 12.23 Å along [100] direction, which allows a facile cleavage into thin belts or nano-membranes [9, 20]. So in this work, we mechanically exfoliated large-scale β-Ga_2O_3 from low dislocation density bulk substrate, and for the first time, the thermally stable Molybdenum (Mo) was chosen as the anode electrode metal to fabricate the β-Ga_2O_3 vertical Schottky barrier diodes.

* Correspondence: qfeng@mail.xidian.edu.cn; jchzhang@xidian.edu.cn
State Key Discipline Laboratory of Wide Band Gap Semiconductor Technology, School of Microelectronics, Xidian University, Xi'an 710071, China

The electrical conduction mechanism under the reverse bias was discussed at the temperature range from 298 to 423 K. This work provides insights into carrier transport mechanisms that can help improve functionalities of β-Ga_2O_3-based devices.

Methods/Experimental

As shown in Fig. 1a, b, the Schottky barrier diode was fabricated on the β-Ga_2O_3 (100) film mechanically exfoliated from the Sn-doped β-Ga_2O_3 substrate, with the thickness of 15 μm and electron concentration of 2×10^{17} cm^{-3}. As presented in Fig. 1d, e, the full width at half-maximum (FWHM) and root mean square (RMS) were estimated to be 51.9 arcsec and 0.19 nm, respectively, by high resolution X-ray diffraction (HRXRD) and atomic force microscope (AFM) measurements. Excellent crystal quality and smooth surface were confirmed by the measurement. After wet chemical cleaning, the Ti/Au (20 nm/100 nm) metal stack was deposited using E-beam evaporation on the back side and followed by the rapid thermal annealing (RTA) at 600 °C for 60 s under nitrogen atmosphere to form the Ohmic contact. The circular Schottky anode electrodes with diameters of 100 μm were formed on the front side by evaporation of Mo/Au (40 nm/100 nm) metals and lift-off process. Figure 1c shows the structure of the schematic cross section of the β-Ga_2O_3 SBD in this work.

Results and Discussion

The current-voltage (I-V) characteristics of Au/Mo/β-Ga_2O_3 Schottky barrier diodes were investigated using a Keithley 4200 semiconductor characterization system between 298 and 423 K. As shown in Fig. 2a, the I_{on}/I_{off} ratio is close to 10^{10} at 298 K, indicating a good rectifying behavior. For the forward bias from 0.1 to 0.7 V, the semilogarithmic I-V curves are almost liner and display a strong temperature dependence behavior. With the forward bias further increasing, the deviation from linearity of the I-V curves is ascribed to the series resistance of the Schottky barrier diode and the relationship between the applied voltage and the current can be expressed as $I = I_s\{\exp[\frac{q(V-IR_s)}{nkT}]-1\}$ [21–23], where V is the applied voltage, R_s the series resistance, T the absolute temperature, k the Boltzmann constant, n the ideality factor, and I_s is the reverse saturation current. The n and I_s can be determined from the slope and intercept of the lnI-V plots, respectively. For the ideal Schottky barrier diode, the ideality factor n should be equal to unity. The higher the n, the greater the deviation from the thermal emission (TE) model. In addition, according to the equation $\phi_b = \frac{kT}{q}\ln[\frac{AA^*T^2}{I_s}]$ [21–23], the values of ϕ_b at different temperatures were also determined, as shown in Fig. 2b, where ϕ_b is the barrier height, A is the diode area and A^* is the effective Richard constant 40.8 A cm^{-2} K^{-2} with the β-Ga_2O_3 effective mass of $m^* = 0.34\ m_0$ [5, 24]. With temperature increasing from 298 to 423 K, the ϕ_b increases while n decreases, indicating another transport mechanism also contributing to the current transport and leading to the deviation of the I-V characteristics from the pure TE model, which has been reported previously in β-Ga_2O_3 Schottky barrier diodes [25] and other wide bandgap devices [26–30]. The barrier height inhomogeneity analysis can be described by a Gaussian distribution in barrier heights,

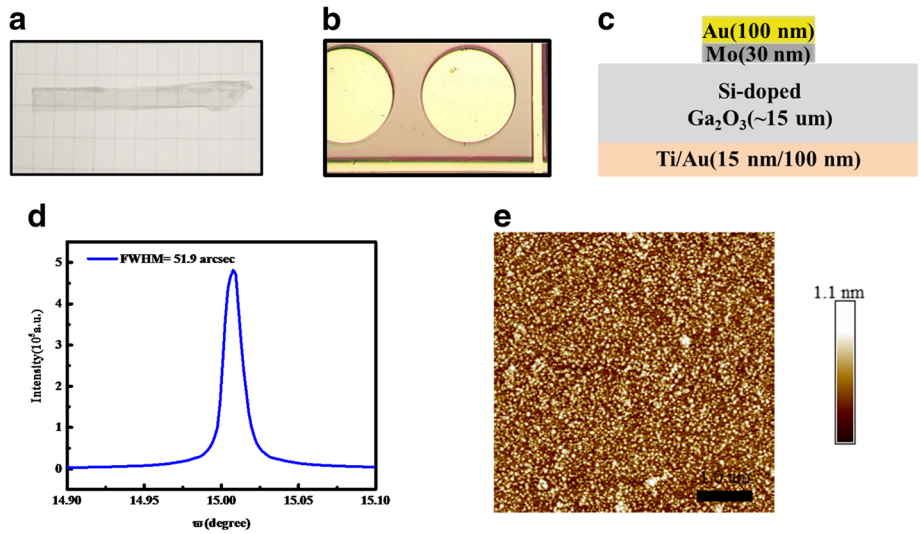

Fig. 1 **a** The Sn-doped β-Ga_2O_3 substrate with the thickness of 300 μm. **b** The Schottky anode electrodes formed on the front side with diameters of 100 μm. **c** The structure of the schematic across section of the β-Ga_2O_3 SBD. **d** XRD rocking curve and **e** AFM image of the β-Ga_2O_3 drift layer mechanically exfoliated from (100) β-Ga_2O_3 substrate

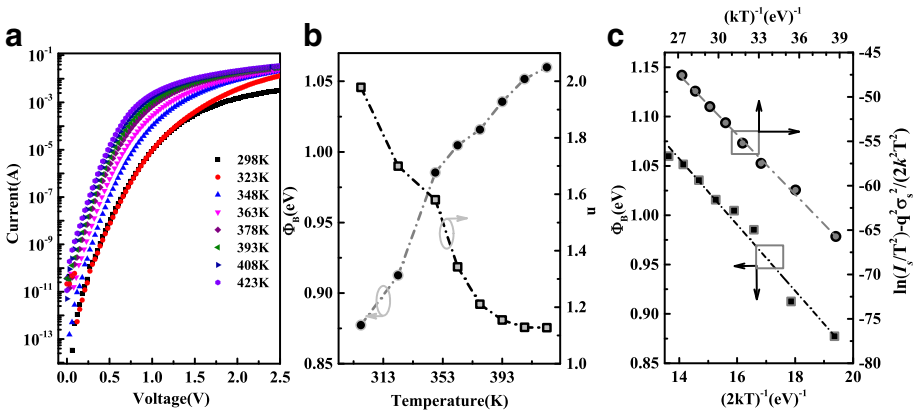

Fig. 2 **a** Forward I-V characteristics of Mo/β-Ga_2O_3 Schottky barrier diodes at different temperatures. **b** Temperature dependence of the ideality factor and Schottky barrier height of β-Ga_2O_3 Schottky barrier diode. **c** Plots of φ_{ap} versus q/2*kT* and modified Richardson plot versus 1/*kT* for the β-Ga_2O_3 Schottky barrier diodes

$$\phi_b = \overline{\phi_{b0}}(T=0) - \frac{q\sigma_s^2}{2kT} \tag{1}$$

The values of mean barrier height $\overline{\phi_{b0}}$ and the standard deviation σ_s are extracted to be 1.55 eV and 0.186 eV, respectively, from Fig. 2c. Furthermore, considering the barrier height inhomogeneities, the conventional Richardson plot is modified as follows:

$$\ln\left(\frac{I_s}{T^2}\right) - \left(\frac{q^2\sigma_s^2}{2k^2T^2}\right) = \ln(AA^*) - \frac{q\overline{\phi_{b0}}}{kT} \tag{2}$$

As shown in Fig. 2c, the modified $\ln(I_s/T^2) - (q^2\sigma_s^2/2k^2T^2)$ versus $1/kT$ is a straight line. The intercept of the curve is used to obtain the A^* of 44.7 A cm^{-2} K^{-2}, which is very close to the theoretical value of β-Ga_2O_3 of 40.8 A cm^{-2} k^{-2}. Hence, the barrier inhomogeneities at metal/semiconductor interface for β-Ga_2O_3 SBD can be explained by TE with Gaussian distribution of barrier over the SBHs.

The room temperature reverse breakdown measurement was also carried out by using Agilent B1505A high-voltage semiconductor analyzer system, as shown in Fig. 3. The breakdown voltage was 260 V while it was 300 V with the sample submerged in Fluorinert ™ produced by 3M company which can prevent air breakdown under high reverse bias. In order to understand the distribution of the electric field, numerical simulation was performed with ATLAS software, as shown in Fig. 4a, b. With the distance increasing from the interface between the semiconductor and the anode to about 1 μm, the electric field gradually decreasing. At the position of x = 4 μm, the average electric field is 3 MV/cm, calculated from Fig. 4c. Also shown in Fig. 4d, at the position of y = 1 nm, the maximum electric field at breakdown voltage was about 8 MV/cm at the edge of the Schottky contact, which is about 2.7 times that of the average electric field. As reported by A. J. Green et al [31] and K. Zeng et al [32], the peak electric field and the average electric field of the electrode edge were 5.3, 3.8 MV/cm and 6.1, 4.4 MV/cm, respectively, and the peak electric field of Mo/Ga_2O_3 Schottky diode is relatively high. It is supposed that the β-Ga_2O_3 nano-membrane obtained by mechanical exfoliation has a large number of dangling bonds and surface states which will capture electrons to deplete the carriers from anode to cathode under reverse bias [33]. Taken the negative surface charge into account, the simulation result showed the electric field at the edge of the Schottky contact reduced with negative surface charge densities increasing from 0.5×10^{13} cm^{-2} to 3×10^{13} cm^{-2}, respectively. Especially with the negative surface charge densities of 3×10^{13} cm^{-2}, the peak

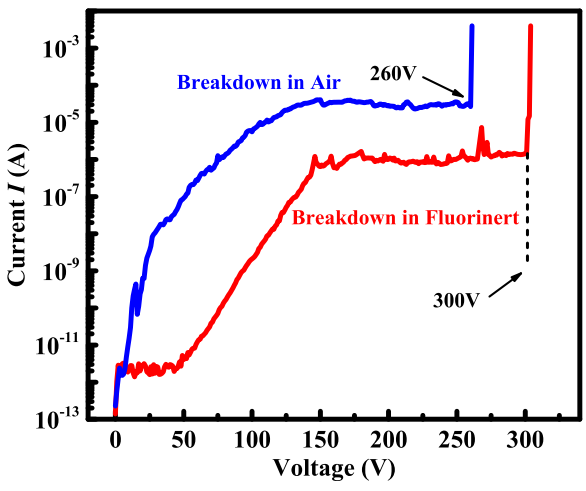

Fig. 3 The reverse I-V characteristics of the β-Ga_2O_3 samples at room temperature respectively in Fluorinert and air

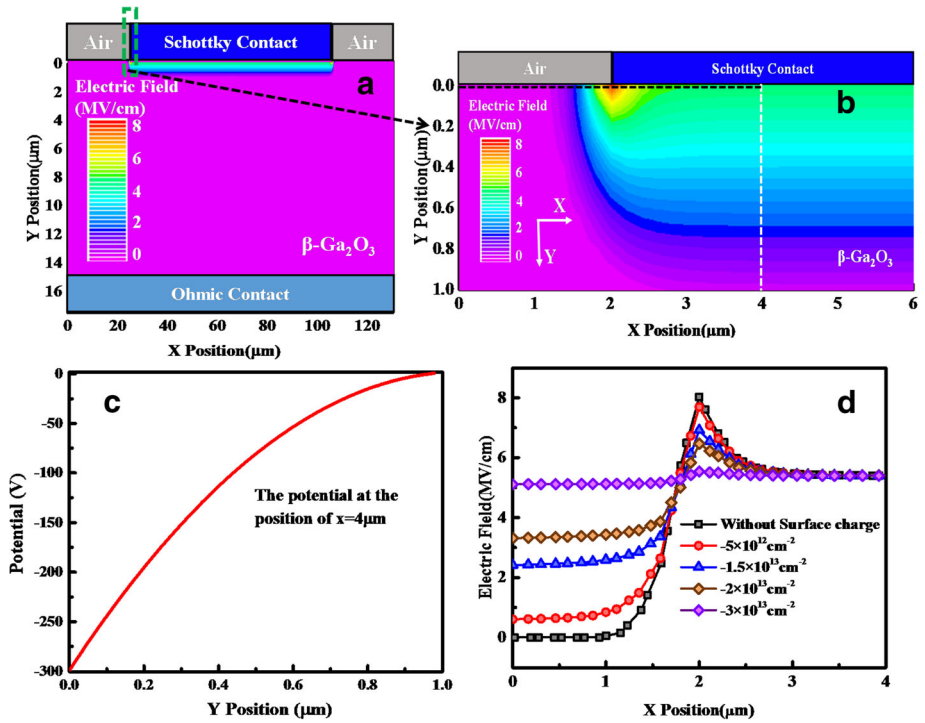

Fig. 4 **a** Off-state TCAD electric field simulation of the Schottky barrier diodes under − 300 V bias. **b** The electric field simulation of the selected regions in green dashed box. The potential along the *y* axis at $x = 4$ μm is present in (**c**), and the electric field at the edge of the Schottky contact reduced with different effective negative surface charge densities are present in (**d**)

electric field at the edge of the Schottky contact is about 5.2 MV/cm. Therefore, the reverse breakdown voltage 300 V can be achieved on the β-Ga_2O_3 nano-membrane with $N_D = 3 \times 10^{17}$ cm^{-2} without any edge termination structures. As shown in Fig. 4d,because of the existence of interface state at *X*-position below 2 μm, the electrons can be trapped and the depletion region can be formed, resulting in the electric field in the *Y* direction. As the interface state concentration increases, the electric field in the *Y* direction increases, although the electric field in the *X* direction approaches zero. So the electric field increases at *X*-position below 2 μm.

On the other hand, with the reverse bias V_{re} increasing, the leakage current I_{re} increases rather than saturate for $|V| > 3\ k_BT/q$, as shown in Fig. 5a, which is inconsistent with the TE theory. Therefore, the electric-field enhanced thermionic emission was considered to discuss the dependence of the I_{re} on V_{re}, including Poole–Frenkel emission and Schottky emission [34, 35]. In Poole–Frenkel emission, the electrons transport from metal into the semiconductor via a trapped state and the I_{re} is given by

$$I_{re} \propto E \exp\left(\frac{q}{kT}\sqrt{\frac{qE}{\pi\varepsilon_S}}\right) \tag{3}$$

while in Schottky emission, the electrons will gain enough energy to overcome the barrier at the metal/semiconductor to form the current and the I_{re} can be expressed by

$$I_{re} \propto T^2 \exp\left(\frac{q}{2kT}\sqrt{\frac{qE}{\pi\varepsilon_S}}\right) \tag{4}$$

where ε_s is the permittivity of the β-Ga_2O_3 ($\sim 10\ \varepsilon_0$) and E is the applied electric field, calculated by $E = \sqrt{\frac{2qN_D}{\varepsilon_S}\left(V + V_{bi} - \frac{k_BT}{q}\right)}$, N_D is the donor density of the β-Ga_2O_3, and V_{bi} is the built-in potential. As shown in Fig. 5b, N_D and V_{bi} can be extracted from the slope and the intercept of the inverse square capacitance ($1/C^2$) versus the V_{re} plots using the following expression

$$\frac{1}{C^2} = \frac{2(V_{\mathrm{bi}} - kT/q - V)}{q\varepsilon_s A^2 N_D} \tag{5}$$

If the curve of $ln(I/T^2)$ versus $E^{1/2}$ is linear, the Schottky emission mechanism is dominant. And if the plot of $ln(I/E)$ versus $E^{1/2}$ is liner, the Poole–Frenkel emission dominates the reverse current transport. Figure 5c, d depicts the plots of $ln(I/E)$ and $ln(I/T^2)$ versus $E^{1/2}$, respectively. Both sets of the curves are linear, indicating not only the Poole–Frenkel emission

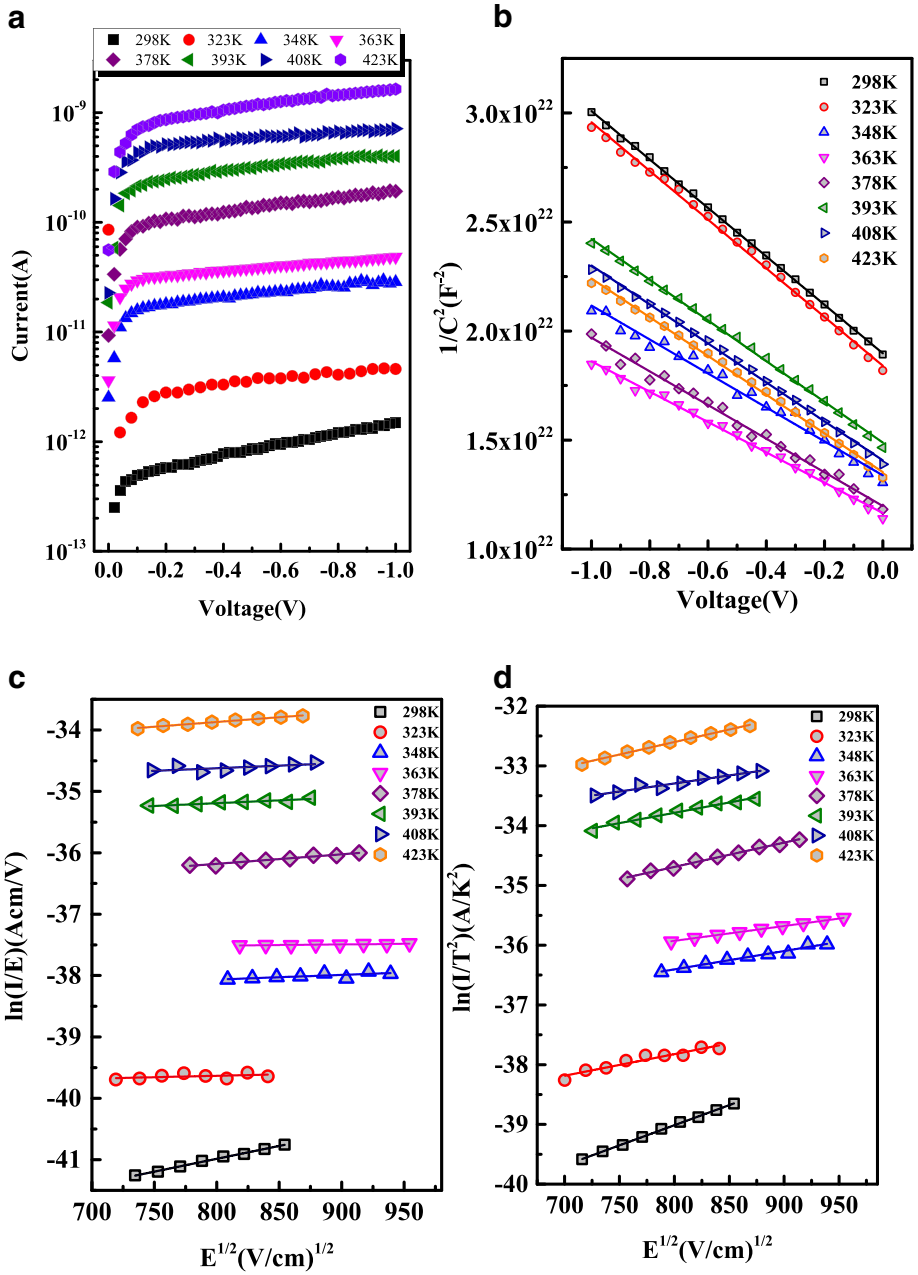

Fig. 5 **a** Reverse I-V characteristics of Mo/β-Ga_2O_3 Schottky barrier diodes at different temperature. **b** Temperature dependence of $1/C^2$ characteristics of the Mo/ β-Ga_2O_3 Schottky barrier diodes. The electric field dependence analysis of Mo/β-Ga_2O_3 Schottky contact with different mechanism. **c** Poole–Frenkel mechanism (I/E) versus $E^{1/2}$ and **d** Schottky mechanism $ln(I/T^2)$ versus $E^{1/2}$

but also the Schottky emission are present. In order to clarify the dominant carrier transport mechanism, the slope of the curves, or the emission coefficient can be expressed as [34–36].

$$S = \frac{q}{nkT}\sqrt{\frac{q}{\pi\varepsilon}} \tag{6}$$

where $n = 1$ is for the Poole–Frenkel emission (S_{PF}) and $n = 2$ for the Schottky emission (S_S). The experimental values of S are denoted as $S_{m\text{-}PF}$ and $S_{m\text{-}S}$ for Poole–Frenkel and Schottky emission given by the slope of the curves in Fig. 5c, d, respectively. The ratios of the experimental value to the theoretical value, N_{PF} ($=S_{m\text{-}PF}/S_{PF}$) and N_S ($=S_{m\text{-}S}/S_S$), are shown in Fig. 6. Since the values of N_S are closer to unity than those of N_{PF}, the reverse current is dominated by the Schottky emission.

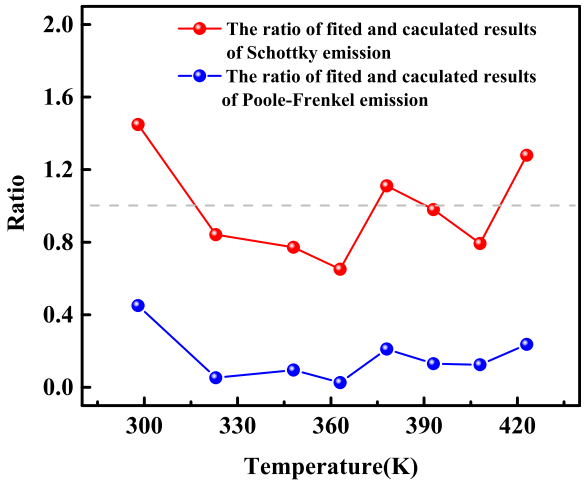

Fig. 6 Relative coefficient plots of Poole–Frenkel emission N_{PF} ($=S_{m\text{-}PF}/S_{PF}$) and Schottky emission N_S ($=S_{m\text{-}S}/S_S$) versus temperature

Conclusions

We have investigated the electrical characteristics of Mo/Au Schottky barrier diodes fabricated on the (100) β-Ga_2O_3 film mechanically exfoliated from the Sn-doped β-Ga_2O_3 substrate. On the basis of TE model, the extracted ϕ_b and n increases and decreases with the increasing temperature, respectively. By assuming the Gaussian distribution of inhomogeneous barrier height, the mean barrier height of 1.55 eV and the standard deviation of 0.186 eV were obtained. Finally, according to the $ln(I/T^2)$ and $ln(I/E)$ versus $E^{1/2}$ plots, the parameter N_S of Schottky emission is close to unity, illustrating the Schottky emission being the dominant transport mechanism of the reverse current. The breakdown voltage of 300 V with samples in Fluorinert is obtained in Mo/Au Schottky barrier diodes with an average electric field of 3 MV/cm, indicating the great potential of β-Ga_2O_3 for power electronics applications.

Abbreviations

I-V: Current-voltage; Mo: Molybdenum; RTA: Rapid thermal annealing; SBD: Schottky barrier diode; TE: Thermionic emission

Acknowledgments

This work was supported by the National ey R&D Program of China (No.2018YFB0406504).

Availability of Data and Materials

The datasets supporting the conclusions of this article are included within the article.

Authors' Contributions

QF and HZ proposed the research work. ZH fabricated and investigated the characteristics of the device, analyze the experiment results, and wrote the paper. ZF and YC carried out the simulation. GY prepared the (100)-oriented β-Ga_2O_3 bulk substrate. All authors helped to correct and polish the manuscript and read and approved the final manuscript.

Competing Interests

The authors declare that they have no competing interests.

Publisher's Note

Received: 17 October 2018 Accepted: 13 December 2018
Published online: 03 January 2019

References

1. Murakami H, Nomura K, Goto K, Sasaki K, Kawara K, Thieu QT, Togashi R, Kumagai Y, Higashiwaki M, Kuramata A (2014) Homoepitaxial growth of β-Ga_2O_3 layers by halide vapor phase epitaxy. Appl Phys Express 8:015503
2. Higashiwaki M, Sasaki K, Kuramata A, Masui T, Yamakoshi S (2012) Gallium oxide (Ga_2O_3) metal-semiconductor field-effect transistors on single-crystal β-Ga_2O_3 (010) substrates. Appl Phys Lett 100:013504
3. Armstrong AM, Crawford MH, Jayawardena A, Ahyi A, Dhar S (2016) Role of self-trapped holes in the photoconductive gain of β-gallium oxide Schottky diodes. J Appl Phys 119:103102
4. Higashiwaki M, Sasaki K, Murakami H, Kumagai Y, Koukitu A, Kuramata A, Masui T, Yamakoshi S (2016) Recent progress in Ga_2O_3 power devices. Semicond Sci Tech 31:034001
5. Sasaki K, Higashiwaki M, Kuramata A, Masui T, Yamakoshi S (2013) Ga_2O_3 Schottky barrier diodes fabricated by using single-crystal Ga_2O_3 (010) substrates. IEEE Electr Device Lett 34:493–495
6. Ahn S, Ren F, Yuan L, Pearton SJ, Kuramata A (2017) Temperature-dependent characteristics of Ni/au and Pt/Au Schottky diodes on β-Ga_2O_3. ECS J Solid State Sc 6:P68–P72
7. Yang J, Ahn S, Ren F, Pearton S, Jang S, Kuramata A (2017) High breakdown voltage (– 201) β-Ga_2O_3 Schottky rectifiers. IEEE Electr Device Lett 38:906–909
8. Splith D, Müller S, Schmidt F, Von Wenckstern H, van Rensburg JJ, Meyer WE, Grundmann M (2014) Determination of the mean and the homogeneous barrier height of Cu Schottky contacts on heteroepitaxial β-Ga_2O_3 thin films grown by pulsed laser deposition. Phys Status Solidi A 211:40–47
9. Zhou H, Si M, Alghamdi S, Qiu G, Yang L, Ye PD (2017) High-performance depletion/enhancement-mode β-Ga_2O_3 on insulator (GOOI) field-effect transistors with record drain currents of 600/450 mA/mm. IEEE Electron Device Lett 38:103–106
10. Farzana E, Zhang Z, Paul PK, Arehart AR, Ringel SA (2017) Influence of metal choice on (010) β-Ga_2O_3 Schottky diode properties. Appl Phys Lett 110:202102
11. He Q, Mu W, Dong H, Long S, Jia Z, Lv H, Liu Q, Tang M, Tao X, Liu M (2017) Schottky barrier diode based on β-Ga_2O_3 (100) single crystal substrate and its temperature-dependent electrical characteristics. Appl Phys Lett 110:093503
12. Tadjer MJ, Wheeler VD, Shahin DI, Eddy CR, Kub FJ (2017) Thermionic emission analysis of TiN and Pt Schottky contacts to β-Ga_2O_3. ECS J Solid State Sc 6:P165–P168
13. Higashiwaki M, Konishi K, Sasaki K, Goto K, Nomura K, Thieu QT, Togashi R, Murakami H, Kumagai Y, Monemar B (2016) Temperature-dependent capacitance–voltage and current–voltage characteristics of Pt/Ga_2O_3 (001) Schottky barrier diodes fabricated on n-Ga_2O_3 drift layers grown by halide vapor phase epitaxy. Appl Phys Lett 108:133503
14. Mohamed M, Irmscher K, Janowitz C, Galazka Z, Manzke R, Fornari R (2012) Schottky barrier height of Au on the transparent semiconducting oxide β-Ga_2O_3. Appl Phys Lett 101:132106
15. Irmscher K, Galazka Z, Pietsch M, Uecker R, Fornari R (2011) Electrical properties of β-Ga_2O_3 single crystals grown by the Czochralski method. J Appl Phys 110:063720
16. Oishi T, Koga Y, Harada K, Kasu M (2015) High-mobility β-Ga_2O_3 single crystals grown by edge-defined film-fed growth method and their Schottky barrier diodes with Ni contact. Appl Phys Express 8:031101
17. Zhang Z, Farzana E, Arehart A, Ringel S (2016) Deep level defects throughout the bandgap of (010) β-Ga_2O_3 detected by optically and thermally stimulated defect spectroscopy. Appl Phys Lett 108:052105
18. Jayawardena A, Ahyi AC, Dhar S (2016) Analysis of temperature dependent forward characteristics of Ni/β-Ga_2O_3 Schottky diodes. Semicond Sci Tech 31:115002
19. Yao Y, Gangireddy R, Kim J, Das KK, Davis RF, Porter LM (2017) Electrical behavior of β-Ga_2O_3 Schottky diodes with different Schottky metals. J Vac Sci Technol B 35:03D113

20. Hu Z, Zhou H, Dang K, Cai Y, Feng Z, Gao Y, Feng Q, Zhang J, Hao Y (2018) Lateral $\beta $-$Ga_2O_3$ Schottky barrier diode on sapphire substrate with reverse blocking voltage of 1.7 kV, IEEE journal of the electron devices. Society 6:815–820
21. Sze SM (1981) Physics of semiconductor devices, 2nd ed. Wiley, New York Chap. 5
22. Cowley A, Sze S (1965) Surface states and barrier height of metal-semiconductor systems. J Appl Phys 36:3212–3220
23. Cheung S, Cheung N (1986) Extraction of Schottky diode parameters from forward current-voltage characteristics. Appl Phys Lett 49:85–87
24. He H, Orlando R, Blanco MA, Pandey R, Amzallag E, Baraille I, Rérat M (2006) First-principles study of the structural, electronic, and optical properties of Ga_2O_3 in its monoclinic and hexagonal phases. Phys Rev B 74:195123
25. Oh S, Yang G, Kim J (2017) Electrical characteristics of vertical Ni/β-Ga_2O_3 schottky barrier diodes at high temperatures. ECS J Solid State Sc 6:Q3022–Q3025
26. Perevalov TV, Shaposhnikov A, Gritsenko VA, Wong H, Han J, Kim C (2007) Electronic structure of α-Al_2O_3: ab initio simulations and comparison with experiment. JETP Lett 85:165–168
27. Ma X, Sadagopan P, Sudarshan TS (2006) Investigation on barrier inhomogeneities in 4H-SiC Schottky rectifiers. Phys Status Solidi A 203:643–650
28. Ewing D, Porter L, Wahab Q, Ma X, Sudharshan T, Tumakha S, Gao M, Brillson L (2007) Inhomogeneities in Ni/4 H-Si C Schottky barriers: localized Fermi-level pinning by defect states. J Appl Phys 101:114514
29. Subramaniyam N, Sopanen M, Lipsanen H, Hong C-H, Suh E-K (2011) Inhomogeneous barrier height analysis of (Ni/Au)–InAlGaN/GaN Schottky barrier diode. Jpn J Appl Phys 50:030201
30. Shin J-H, Park J, Jang S, Jang T, Sang Kim K (2013) Metal induced inhomogeneous Schottky barrier height in AlGaN/GaN Schottky diode. Appl Phys Lett 102:243505
31. Green AJ, Chabak KD, Heller ER, Fitch RC, Baldini M, Fiedler A, Irmscher K, Wagner G, Galazka Z, Tetlak SE, Crespo A, Leedy K, Jessen GH (2016) 3.8-MV/cm breakdown strength of MOVPE-grown Sn-doped β-Ga_2O_3 MOSFETs. IEEE Electron Device Lett 37:902–905
32. Zeng K, Vaidya A, Singisetti U (2018) 1.85 kV breakdown voltage in lateral field-plated Ga_2O_3 MOSFETs. IEEE Electron Device Lett 39:1385–1388
33. Hu Z, Zhou H, Feng Q, Zhang J, Zhang C, Dang K, Cai Y, Feng Z, Gao Y, Kang X, Hao Y (2018) Field-plated lateral β-Ga_2O_3 Schottky barrier diode with high reverse blocking voltage of more than 3 kV and high DC power figure-of-merit of 500 MW/cm^2. IEEE Electron Device Lett 39:1564–1567
34. Lee H-D (2000) Characterization of shallow silicided junctions for sub-quarter micron ULSI technology. Extraction of silicidation induced Schottky contact area. IEEE T Electron Dev 47:762–767
35. Janardhanam V, Kumar AA, Reddy VR, Reddy PN (2009) Study of current–voltage–temperature (I-V-T) and capacitance–voltage–temperature (C-V-T) characteristics of molybdenum Schottky contacts on n-InP (100). J Alloy Compd 485:467–472
36. Janardhanam V, Jyothi I, Ahn K-S, Choi C-J (2013) Temperature-dependent current–voltage characteristics of Se Schottky contact to n-type Ge. Thin Solid Films 546:63–68